Photoexcitation and One-Electron Reduction Processes of a CO_2 Photoreduction Dyad Catalyst Having a Zinc(II) Porphyrin Photosensitizer

Teruyuki Honda[1], Takumi Ehara[1], Ren Sato[2], Tomohiro Ogawa[1], Yusuke Kuramochi[2$], Akiharu Satake[2], Kiyoshi Miyata[1]*, Ken Onda[1]*

[1]Department of Chemistry, Faculty of Science, Kyushu University, 744 Motooka, Nishi-ku, Fukuoka 819-0395, Japan

[2]Graduate School of Sciences, Tokyo University of Science, 1-3 Kagurazaka, Shinjuku-ku, Tokyo 162-8601, Japan

[$]Present address: Institute of Industrial Science, The University of Tokyo, 4-6-1 Komaba, Meguro-ku, Tokyo 153-8505, Japan

*Corresponding authors: kmiyata@chem.kyushu-univ.jp, konda@chem.kyushu-univ.jp

Keywords: CO_2 photocreduction, Zinc (II) porphyrin, Time-resolved infrared spectroscopy, Time-resolved transient absorption spectroscopy

Abstract

We have explored the photophysical properties and one electron reduction process in the dyad photocatalyst for CO_2 photoreduction, **ZnP-phen=Re**, in which the catalyst of *fac*-[Re(1,10-phenanthoroline)$(CO)_3$Br] (**phen=Re**) is directly connected with the photosensitizer of zinc (II) porphyrin (**ZnP**), using time-resolved infrared spectroscopy, transient absorption spectroscopy, and quantum chemical calculations. We revealed the photophysical properties that (1) the intersystem crossing occurs with a time constant of ~20 ps, which is more than 50 times faster than that of zinc (II) porphyrin, and (2) the charge density in the excited singlet and triplet states is mainly localized on ZnP, which means the excited state is assignable to the π -π^* transition in **ZnP**. The one electron reduction using the reductant, 1,3-dimethyl-2-,3-dihydro-1H-benzo[d]imidazole (BIH), occurs via the triplet excited state with time constant of ~170 ns and directly from the ground state by the deprotonated BIH with the time constant of ~3 μs. The charge in the one electron reduction species spans **ZnP** and the phenanthroline ligand and the dihedral angle between **ZnP** and the phenanthroline ligand is rotated by ~24° with respect to that in the ground state, which presumably offers an advantage for proceeding to the next CO_2 reduction reaction step. These findings on the initial processes of CO_2 photoreduction would help us to design novel dyad photocatalysts using porphyrin photosensitizers.

1. Introduction

Toward a sustainable society, CO_2 photoreduction using sunlight, also known as artificial photosynthesis, is one of the most promising approaches to provide clean energy sources[1–3]. With its high demand, many CO_2 photocatalytic reduction reactions have been reported using semiconductors[3], covalent organic frameworks[4], and metal complexes[5]. As an intensively investigated photocatalytic system, a series of dyad catalysts consisting of a $[Ru(diimine)_3]^{2+}$ sensitizer and a *fac*-$[Re(diimine)(CO)_3Cl]$ catalyst connected with an alkyl chain (**Ru-Re**) achieved highly efficient CO formation with a high quantum yield ($\phi_{CO} = 46\%$) and a high turnover number ($TON_{CO} > 2915$)[2,5]. Nevertheless, frequently-used precious metal complexes are not ideal photosensitizers in terms of their photophysical properties as well as their costs[6].

As photosensitizers, metal porphyrins have many advantages such as high absorption coefficients and visible-light absorption[7], and they typically consist of earth-abundant elements. In fact, natural photosynthesis uses magnesium porphyrin derivatives known as chlorophyll for photosensitization[7,8]. Dyad metal complex systems for CO_2 photoreduction using a metal porphyrin photosensitizer have also been developed[9–15]. There are several reports on the dyad photocatalysts composed of zinc (II) porphyrin and $[Re(diimine)(CO)_3Cl]$. Gabrielsson et al. reported the dyad photocatalyst in which a zinc (II) porphyrin and a fac-$[Re(bpy)(CO)_3Cl]$ (bpy=2,2'-bipyridine) are connected by a saturated methylene spacer in the amide-bridge linker[10]. This dyad catalyst attained TON_{CO} of 260 for CO production. Matlachowski, at al. reported that the rigid xanthene-bridged dyad of a zinc (II) porphyrin and $[Re(bpy)(CO)_3Cl]$ showed TON_{CO} of 200[11]. Despite those developments, one of the major issues is low TON_{CO} because porphyrin

photosensitizers have relatively less chemical stability; porphyrins tend to be decomposed by hydrogenation of the C=C bonds during photoirradiation[12,13].

Recently, a dyad photocatalyst with direct connection of a zinc (II) porphyrin (**ZnP**) and a *fac*-[Re(phenanthroline)$(CO)_3$Br] (**ZnP-phen=Re,** Figure 1)[16,17] significantly improved the performance of ϕ_{CO} (= 8%), TON_{CO} (> 1300), and CO selectivity (>99.9%). The long lifetime of the lowest triplet state (T_1) allowed an efficient quenching with an electron donor, which exhibited a high Stern-Volmer constant K_{sv} = 180 000 M^{-1}. It was hypothesized that one electron-reduced ZnP efficiently transfers an electron to the Re catalyst moiety (**phen=Re**). This efficient electron transfer from the zinc (II) porphyrin to the Re catalyst likely suppresses the electron accumulation on the porphyrin because electron accumulation is known as a possible decomposition pathway of the porphyrin[12,13,16,18].

Scheme 1 shows the initial process prior to CO_2 reduction reaction assumed in the previous work.[17]. After photoexcitation, the lowest excited singlet state (S_1) is formed in **ZnP** (process 1), and S_1 undergoes intersystem crossing to T_1 (process 2). T_1 is quenched by 1,3-dimethyl-2-,3-dihydro-1*H*-benzo[*d*]imidazole (BIH)[19] and one-electron reduced species (OERS) is generated. The electron on **ZnP** moves to **phen=Re** (process 3). Those processes are followed by the catalytic cycle. In this dyad, it is expected that the two units are close enough to have an interaction between the two units that would affect electron/structure properties. However, the properties of each process have never been quantitatively examined, such as the rate constant of each process or the structure and electron distribution in each excited state. In order to reveal the modulation in excited state dynamics on the Zn porphyrin in the presence of the connection to the Re complex and the loss process governing the total quantum efficiency, it is necessary to investigate each process in the molecular level in realtime.

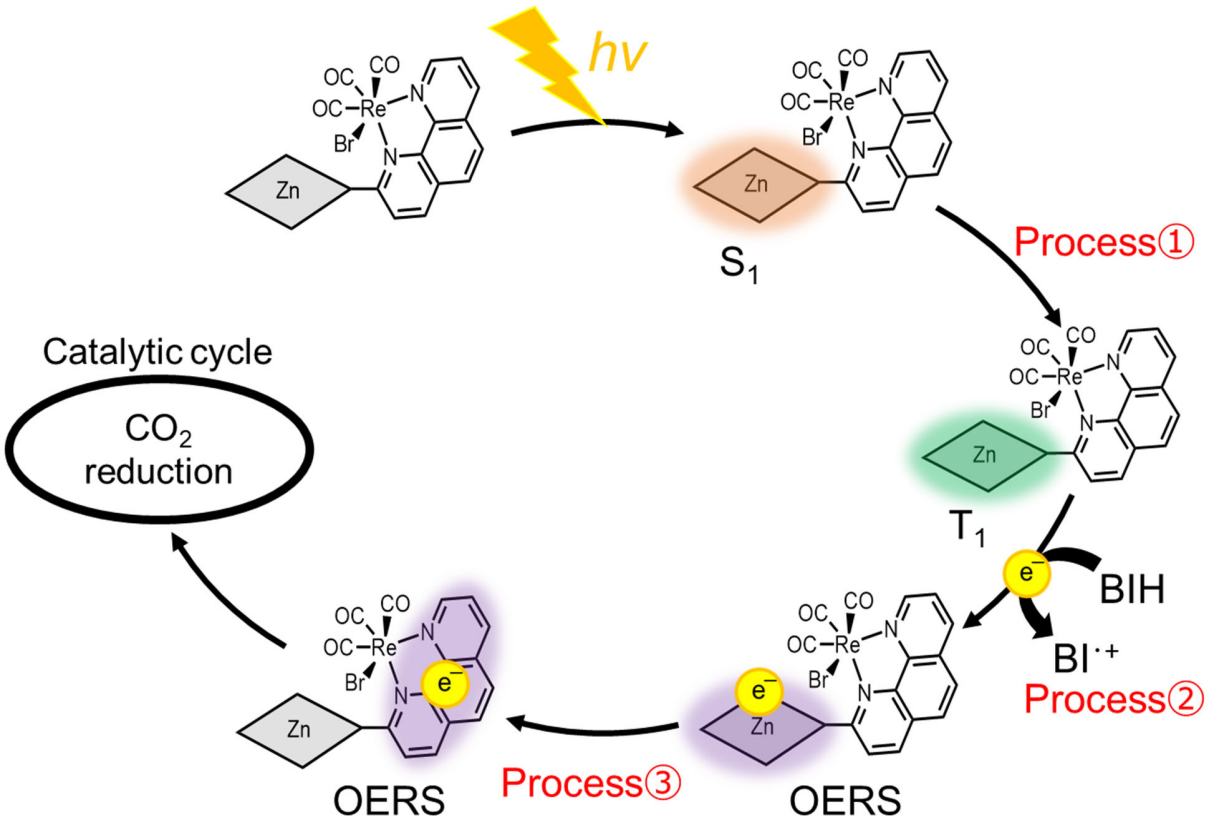

Scheme 1. Predicted mechanism on the formation of OERS in the photocatalytic CO_2 reduction reaction using **ZnP-phen=Re**.

Time-resolved infrared spectroscopy (TR-IR) is an ideal tool for quantifying the multi-step processes of CO_2 photoreduction. TR-IR allows us to obtain the information on changes in the electron density of central metal in a metal carbonyl complex by monitoring the CO stretching vibrations. Also, TR-IR allows us to obtain the information on the metal-to-ligand charge transfer and metal center transitions by measuring the vibrations in the fingerprint region[20–22]. We previously investigated the processes of **Ru-Re** behind the formation of the OERS and its reactivity using TR-IR in the presence of BIH and triethanolamine (TEOA)[5,23], and almost all the processes in **Ru-Re** CO_2 photoreduction systems have been revealed[5,24,25]. In the previous works, OERS was generated via the two processes: (i) the reductive quenching of the excited Ru unit by

BIH following intramolecular electron transfer from the Ru unit to the Re unit, and (ii) the reduction of **Ru-Re** in the ground state by BI· produced by deprotonation in the process (i). The time constants of processes (i) and (ii) were several tens of nanoseconds and several microseconds, respectively. It is essential to reveal how those processes were affected by the porphyrin-based systems.

In this paper, we investigated the initial processes of CO_2 photoreduction reaction of **ZnP-phen=Re** and the photophyical properties of **ZnP** for reference (**Figure 1.** Molecule structures of **ZnP-phen=Re** and **ZnP**.Figure 1) using TR-IR as well as Vis-NIR transient absorption (TA) spectroscopy and quantum chemical calculations. We succeeded in (1) observing the intersystem crossing with a time constant of ~20 ps, which is more than 50 times faster than that of zinc (II) porphyrin alone, (2) detecting small redshifts of CO stretching vibration peaks in S_1 and T_1, indicating π-π* transition in ZnP and slight structural distortion, (3) determining the two pathways for OERS generation in the presence of BIH reductatnt: the ~170 ns reduction by BIH and the ~3 μs reduction by BI·. Under the CO_2 atmosphere, the same spectral changes were observed as those without CO_2, indicating that the reaction between **ZnP-phen=Re** and CO_2 occurs later than 1 ms. Our discovery disentangled the perturbation on the electronic properties of **ZnP** caused by the presence of the Re catalyst and vice versa.

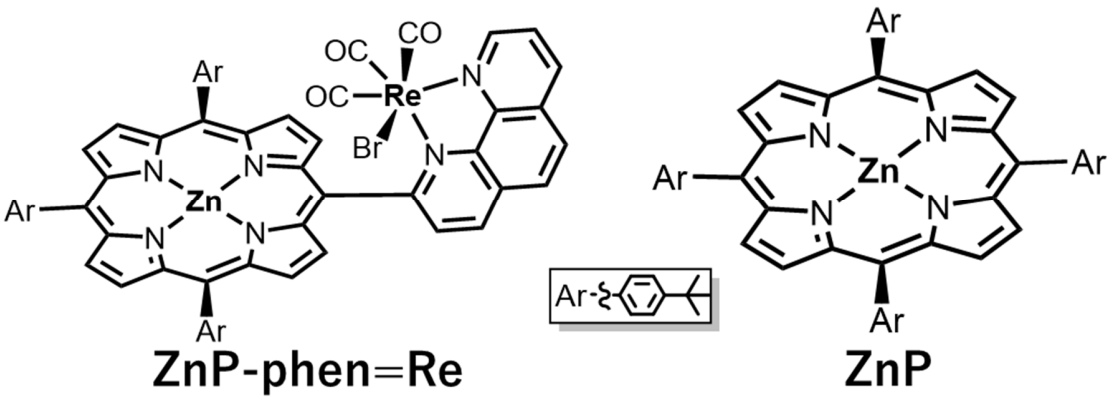

Figure 1. Molecule structures of **ZnP-phen=Re** and **ZnP**.

2. Experimental

A. Materials

The complexes, **ZnP-phen=Re** and **ZnP**, were synthesized according to the previous report[16,17]. The reductant, BIH, was synthesized according to the previous report[19]. The solvent, N,N-dimethylacetamide (DMA), was purchased from Kanto Chemical Co.

B. Fourier transform infrared spectroscopy (FT-IR)

The steady-state IR absorption spectra were measured using a Fourier transform infrared spectrometer (Perkin-Elemer, Spectrum 3, wavenumber resolution ~4 cm^{-1}). The sample solutions were sealed in a home-built infrared cell equipped with BaF_2 windows with an optical path length 0.5 mm. The concentration of sample solutions was 0.3 mM in DMA.

C. Transient absorption spectroscopy (TA)

TA measurements were carried out by the pump-probe methods. For the probe pulse, a white light pulse (460 nm -720 nm) was generated by focusing a part of the output of Ti:sapphire regenerative amplifier (Spectra-Physics, Spitfire Ace, central wavelength = 800 nm, pulse duration ~120 fs, repetition rate = 1 kHz, pulse energy = 3.5 mJ/pulse) on a sapphire crystal (3 mm thickness). For the pump pulse in the picosecond range up to 1 ns delay time, the 400 nm sub-picoscond pulase was generated by second harmonic generation using a BBO (β-BaB_2O_4) crystal from the other part of the output of amplifier. The fluence of pump pulse at the sample position was 0.94 mJ/cm^2. For the pump pulse after 1 ns delay time, the 410 nm nanosecond pulse was obtained from the optical parametric oscillator pumped by third harmonic generation of Nd:YAG laser (EKSPLA NT242, pulse duration ~ 3 ns, repetition rate = 1 kHz) synchronized with the amplifier using a picosecond

delay generator (Stanford Research Systems, DG535). The polarization of the pump and probe pulses were set to the magic-angle configuration (~54.7°). The probe pulse which passed through the sample solution was dispersed by a polychromator (JASCO, CT-10TP, 300 grooves/500 nm). The spectra were recorded using a multichannel detection system equipped with a CMOS sensor (UNISOKU, USP-PSMM-NP). The concentration of the sample solutions was 0.1 mM in DMA and all measurements except for CO_2 reaction were conducted under nitrogen gas bubbling after 30-minute bubbling with argon gas.

D. Time-resolved infrared spectroscopy (TR-IR)

The experimental setup for the home-built pump-probe TR-IR measurement system has been reported previously [20,21,26–29]. Briefly, a broadband mid-IR probe pulse (pulse duration ~120 fs, bandwidth ~150 cm^{-1}, tunable range = 1000 cm^{-1} - 4000 cm^{-1}) was generated by difference frequency generation between the signal and idler pulses from the optical parametric amplifier (Lighconversion TOPAS-Prime) pumped by the regenerative Ti:sapphire amplifier (Spectra-Physics, Spitfire Ace). The same pump pulses as the TA measurements were used for the pump pulses before and after 1 ns delay time were. The polarization angles of the pulse for the pump and probe were set to the magic angle (54.7°). The sample solutions were continuously circulated through a home-built infrared cell equipped with BaF_2 windows with an optical path length 0.5 mm. A probe pulse passed through an optical cell was dispersed by a 19-cm polychromator followed by detection using a 64-channel mercury-cadmium-telluride (MCT) infrared detector array. The concentration of the sample solutions was 0.1 mM in DMA and and all measurements except for CO_2 reaction were conducted under nitrogen gas bubbling after 30-minute bubbling with argon gas.

E. Quantum Chemical Calculations

Quantum chemical calculations were performed using the Gaussian 16 package Revision C.01[30]. Ground singlet state (S_0), excited singlet state (S_1), excited triplet state (T_1), and doublet states (OERS) were calculated based on density functional theory (DFT), and the S_1 state was calculated based on time-dependent TD-DFT. We employed the LanL2DZ basis set and the ωB97XD functional. Infrared vibrational spectra were calculated based on the optimized geometry for each state. The vibrational spectra were appropriately scaled with the scaling factor to take into account the wavenumber shifts caused by anharmonicity[31].

3. Results and discussion

3.1. Photophysical properties in the excited state

3.1.1. Transient absorption spectroscopy

To investigate the initial excited-state behavior in **ZnP-phen=Re**, we first discuss the TA spectra observed in the picosecond (ps) range. Figure 2(a) shows the TA spectra of **ZnP-phen=Re** in a DMA solution after photoexcitation at 400 nm. Immediately after photoexcitation at 0 ps, the excited state absorptions (ESA) were observed at 500 nm, 600 nm, and 650 nm, and the ground state bleach (GSB) were observed at 575 nm and 630 nm. We conducted the global analysis assuming a sequential model with three components (Figure 2(b)), and obtained the time constants of $\tau_{EAS1} = 0.2 \pm 0.1$ ps, $\tau_{EAS2} = 17 \pm 1.3$ ps, and $\tau_{EAS3} > 1000$ ps (EAS: evolution assisted spectrum). We also conducted the nanosecond to microsecond (ns-μs) TA measurements and revealed that the lifetime of the long-lived species is approximately 100 μs (Figure S1).

We found that the dynamics observed in **ZnP-phen=Re** was unique compared to the typical dynamics in zinc (II) porphyrin systems. EAS2 and EAS3 in **ZnP-phen=Re** display the features corresponding to the TA spectrum of S_1 and T_1 in **ZnP** (Figure S2)[32]. Since quick internal conversion (IC) from S_2 to S_1 typically occurs in less than picoseconds in porphyrin dyad systems [9,33], we reasonably assigned EAS1, EAS2, and EAS3 to the S_2, S_1, and T_1, respectively. Based on these assignments, the time constants of 0.2 ± 0.1 ps and 17 ± 1.3 ps are attributed to IC and intersystem crossing (ISC) from S_1 to T_1, respectively[32,34]. Note that the ISC time constant of 17 ps is approximately 50 times faster than the typical ISC time constants in **ZnP**, 1-2 ns[35]. We hypothesize that the acceleration of ISC is due to enhancement of the spin-orbit coupling by the heavy atom effect of the Re ion located near the **ZnP**.

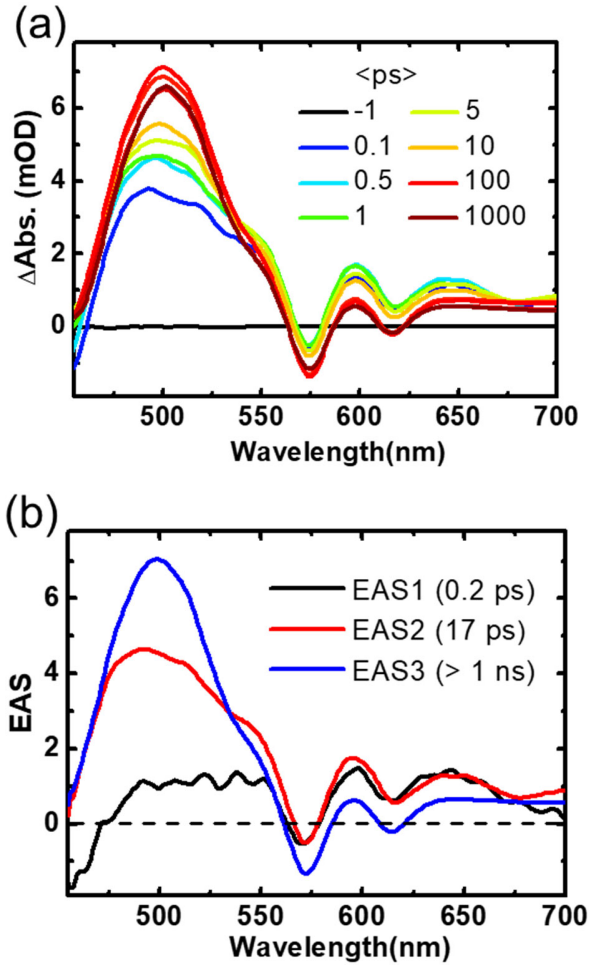

Figure 2. (a) Temporal evolution of TA spectra in the ps range of **ZnP-phen=Re** in a 0.1 mM DMA solution after photoexcitation at 410 nm, and (b) EASs and their time constants obtained from the global analysis of TA data.

3.1.3. Time-resolved Infrared Spectroscopy (TR-IR)

The wavenumber of CO stretching vibrations in a metal carbonyl complex is known to be sensitive to the charge on the central metal of the complex[5,10,12,36,37]. We measured the TR-IR spectra in the ps range in the CO stretching vibrational region, 1850 cm^{-1} - 2050 cm^{-1}, of **ZnP-phen=Re** (Figure 3(a)). Immediately after photoexcitation, GSBs were observed at the same wavenumbers as the peaks in the FT-IR spectra (1890 cm^{-1}, 1917 cm^{-1}, and 2019 cm^{-1}, Figure S3), and ESAs were observed at 2000 cm^{-1} and 1860 cm^{-1}. These red shifts became smaller within 50 ps. We conducted a global analysis assuming a sequential model with two components on the TR-IR data (Figure 3(b)). Since the time constant of EAS1 of 21±2.1 ps was close to that of ISC from S_1 to T_1 estimated from the TA spectra (17±1.3 ps), we assigned EAS1 and EAS2 to S_1 and T_1, respectively. IC from S_2 to S_1 could not be observed in the measurements due to the limitation of the instrumental response function (~200 fs). We also conducted TR-IR in the ns-μs range and confirmed the lifetime of the EAS2 was longer than 10 μs (FigureS4).

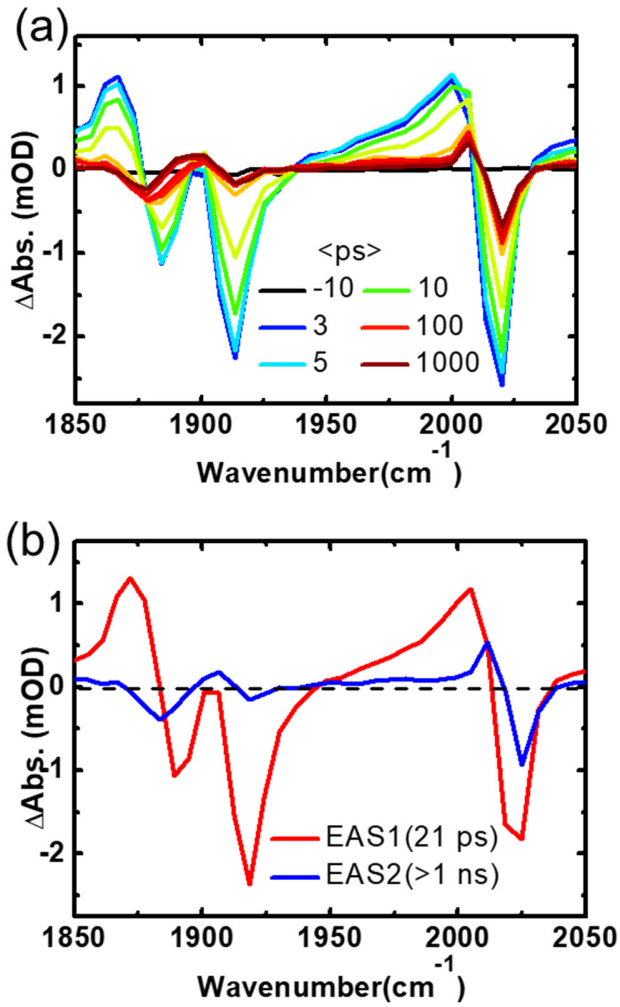

Figure 3. (a) Temporal evolution of TR-IR spectra in the ps range of **ZnP-phen=Re** in a 0.1 mM DMA solution after photoexcitation at 400 nm, and (b) EASs and their time constants obtained from the global analysis of TR-IR data.

To discuss the origin of the peak redshifts of the CO stretching vibrations upon photoexcitation, we quantified the peak positions in the TRIR spectra of S_0, S_1, and T_1 by spectral deconvolution. We assumed that each peak is a gaussian function and fitted the spectra employing the formula below representing overlapping between ESA and GSB,

$$y = y_0 + A1 * e^{-\frac{(\lambda-\lambda_{c1})^2}{w_1^2}} - A2 * e^{-\frac{(\lambda-\lambda_{c2})^2}{w_2^2}} ,$$

where λ_{c1} and λ_{c2} represent the center position of the peaks, respectively, w_1 and w_2 represent the peak widths, repsectively. We conducted the least squares fitting on the TR-IR spectra in the range from 1990 cm^{-1} to 2040 cm^{-1} for S_1 at 3 ps and T_1 at 1000 ps. The results of fitting are summarized in Table 1. The shifts from S_0 are calculated to be -15 cm^{-1} and -7 cm^{-1} for S_1 and T_1, respectively.

Table 1. Center positions determined by multi-Gaussian fit to the TR-IR spectra in the range from 1990 cm^{-1} to 2040cm^{-1} at 3 ps for S_1 and at 1000 ps for T_1, and wavenumber shifts from those in S_0.

	Center position	Shift from S_0
S_0	2019 cm^{-1}	-
S_1	2004 cm^{-1}	-15 cm^{-1}
T_1	2012 cm^{-1}	-7 cm^{-1}

3.1.4. Quantum chemical calculations and spectral simulations of TR-IR spectra

Comparing TR-IR spectra to spectral simulations using quantum chemical calculations allows us to obtain a deeper understanding on excited-state characters in metal complexes[20,28]. We conducted DFT calculations for S_0 and TD-DFT calculations for S_1 and T_1 in **ZnP-phen=Re**. We first calculated the infrared absorption (IR) spectrum of the structure optimized in S_0 and compared it to the FT-IR spectrum measured in a DMA solution in the range of 1850 - 2050 cm^{-1}. We conducted the calculations using several combinations of a basis set and a functional, and adopted the LanL2DZ basis set and the ωB97XD functional, which best reproduces the experimental FT-IR and TR-IR spectra (Figure S5). Since the calculated spectrum reasonably corresponds to the experimental spectrum, we discussed the molecular geometry based on the calculated structure. According to the optimized structure shown in Figure S6(a), the dihedral angle between the **ZnP** plane and the phenanthroline planes is 102°(Figure S6(b)) and the distance between the Re ion and the Zn ion is 5.5 Å (Figure S6(c)), indicating that the Re ion is located just above the **ZnP**. This small distance between the Zn and Re ions must enhance the spin-orbit coupling and accelerates the ISC rate in **ZnP-phen=Re**.

Figure 4(a) shows the calculated difference IR spectrum between S_1 and S_0 (blue line) and the TR-IR spectrum of S_1 measured at 3 ps after photoexcitation (red line) in the CO stretching vibrational region of 1850 cm^{-1} - 2050 cm^{-1}. The calculated difference spectrum well reproduces the TR-IR spectrum, which assures that the calculations are reliable enough to discuss the excited state properties. The S_1 optimized geometry shows that the dihedral angle between the **ZnP** and **phen** planes is 108°, which is slightly larger than that in S_0. The natural transition orbitals (NTOs) of S_1 shown in Figure 4(c) indicate that the transition is mainly attributed to the π-π^* transition in

ZnP with slightly extention of the orbitals toward the phenanthroline. Figure 4(b) shows the calculated difference IR spectrum between T_1 and S_0 (blue line) and the TR-IR spectrum of T_1 measured at 1000 ps after photoexcitation (red line). The NTOs of T_1 show π-π* transition like those of S_1 (Figure 4(d)), and the dihedral angle between the **ZnP** and **phen** plains in the T_1 geometry was 102°, indicating the similarity to the optimized geometry in S_0. Because the dihedral angle corresponds to the degree of π-conjugation across the porphyrin unit and the phenanthroline ligands, we argue that the interaction between the two units in T_1 gets weakened compared to the interaction at the optimized geometry in S_1. This is consistent with the smaller CO peak shift observed in T_1. The picture of S_1 with π-π* excitation of **ZnP** in the dyad system is consistent with the fact that the emission from S_1 can mainly be explained by the emission from **ZnP** with accrelated decay of ~20 ps[38].

In general, the wavenumber shifts of CO stretching vibrations of metal carbonyl complexes upon photoexcitation are thought to originate from the difference in charge on the central metal. However, in the case of **ZnP-phen=Re**, the wavenumber shift is presumed to result mainly from the difference in structure in the vicinity of the Re ion because there is little difference in NTOs on the Re ion between the electronic states.

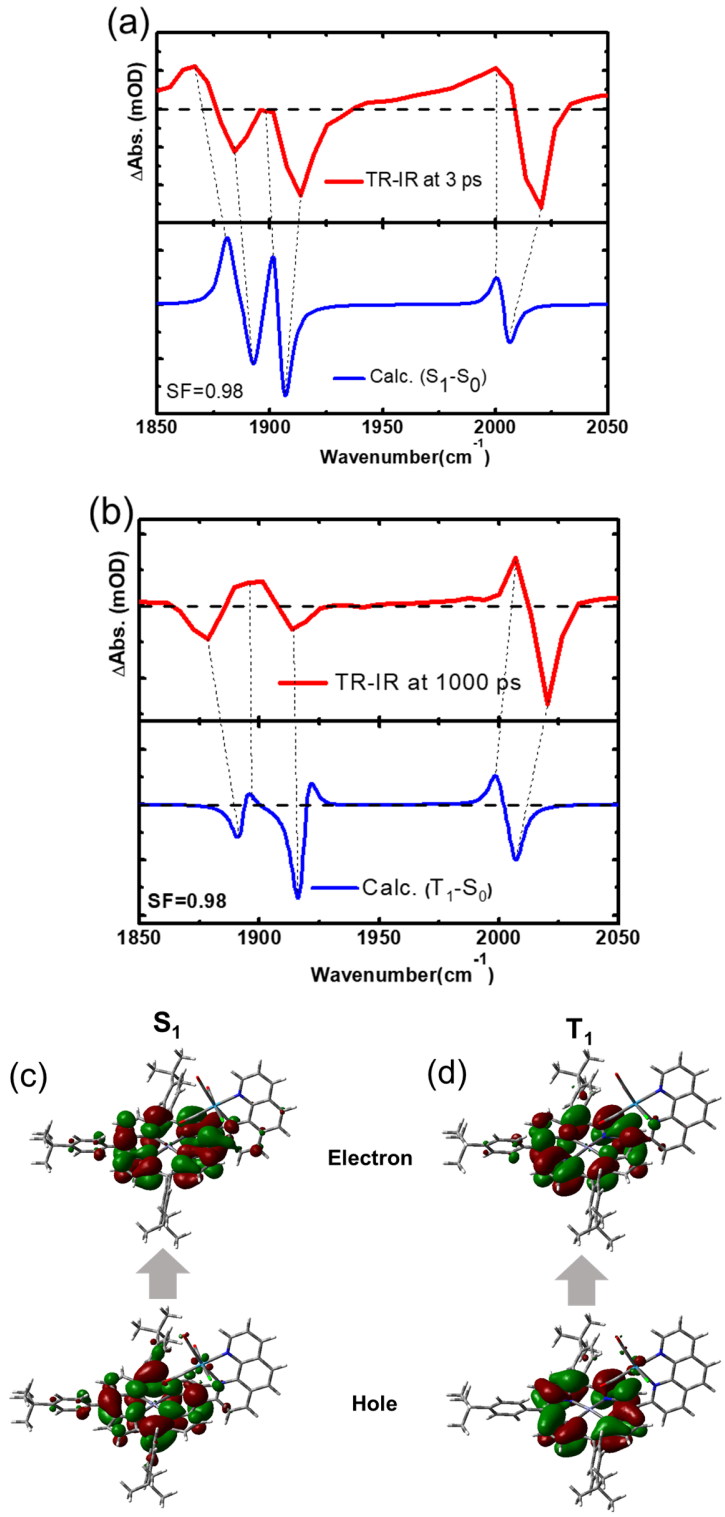

Figure 4. (a) TR-IR spectra at 3 ps (red line) and calculated difference IR spectra between S_1 and S_0 (blue line). (b) TR-IR spectra at 1000 ps (red line) and calculated difference IR spectra between T_1 and S_0 (blue line). (c, d) NTOs for the S_1 and T_1 at the optimized geometries of

3.2. Production and properties of OERS

3.2.1. TA in the presence of BIH

To explore the formation of OERS, we conducted TA measurements of **ZnP-phen=Re** in the presence of an electron donor, BIH. Figure 5(a) shows the TA spectra in the ns-μs range of **ZnP-phen=Re** in a DMA solution with 0.05 M BIH after photoexcitation at 410 nm. At 0 ns, ESAs were observed at 500 nm, 600 nm, and 650 nm and GSBs were observed at 575 nm and 630 nm. Because these ESAs and GSBs are almost the same as the spectrum observed in **ZnP-phen=Re** without BIH (Figure S1(a)), the TA spectrum at around 0 ns is assigned to the T_1 state. Figure 5(b) compares the temporal profiles of TA signals at 495 nm in the presence and absence of BIH. A quick decay component with a time constant of approximately 1-2 μs, followed by a much slower decay component, was observed in the presence of BIH. In addition, the peak position of the ESA at 500 nm showed a red shift associated with the quick decay. This spectral evolution can be attributed to the electron reduction process of **ZnP-phen=Re**.

We conducted a global analysis of the TA spectra, assuming a sequential model with two components (Figure 5(c)). Note that OERS is produced by two processes: reductive quenching of T_1 by BIH and reduction of S_0 by BI· produced via the deprotonation of BIH[19]; thus, the two-component sequential model is a coarse model. Because the shape of EAS2 corresponds to that of electrochemically produced OERS[17], EAS1 and EAS2 are assigned to T_1 and OERS, respectively. The time constant of generation of OERS from these measurements was estimated to be 980±90 ns; as mentioned above this is an apparent value due to the coarse model. Given that the intrinsic lifetime of T_1 was 100 μs, the quantum yield of the electron transfer to T_1 of the dyad is expected to be almost unity at the concentration[39,40].

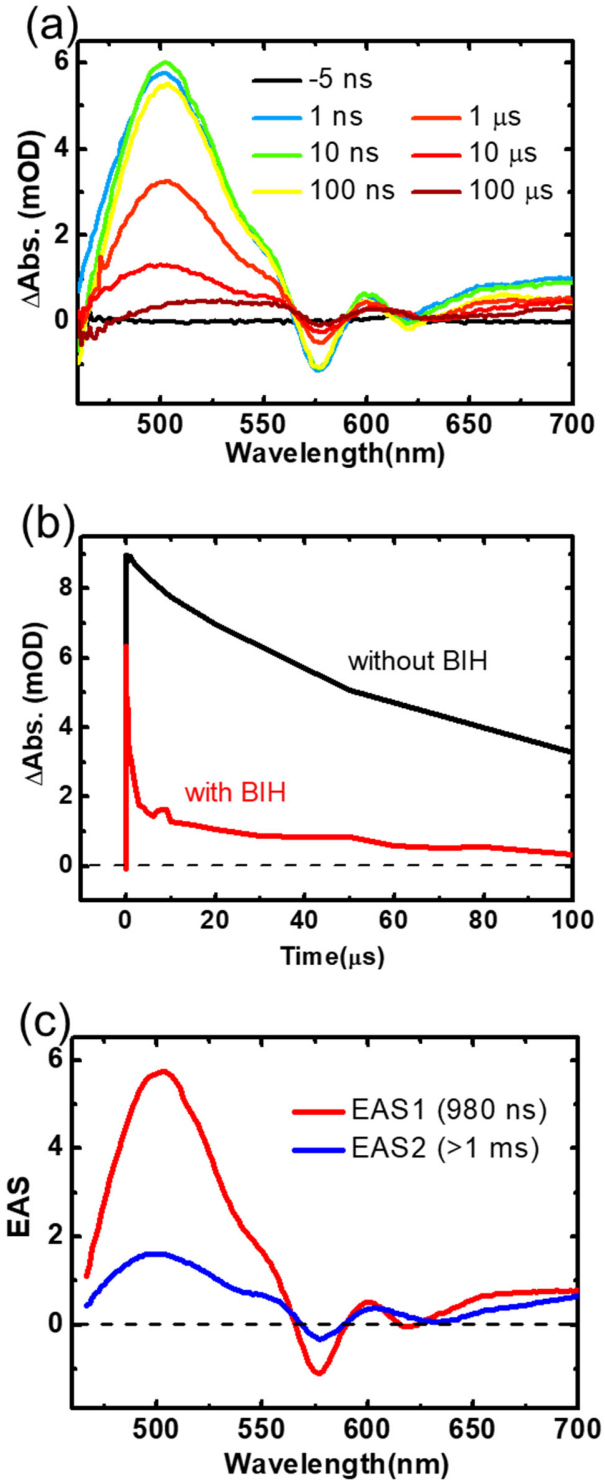

Figure 5. (a) Temporal evolution of TA spectra in the ns-μs range of **ZnP-phen=Re** in a 0.1 mM DMA solution with 0.05 M BIH after photoexcitation at 410 nm. (b) Temporal profiles of TA spectra at 500 nm with BIH (red line) and without BIH (black line). (c) EASs and their time constants obtained from the global analysis of the TA spectra with BIH.

3.2.2. TR-IR in the presence of BIH

For deeper understanding the OERS generation processes, we measured the TR-IR spectra of **ZnP-phen=Re** in a DMA solution in the presence of 0.05 M BIH after photoexcitation at 400 nm (Figure 6(a)). At 0 ns, the two ESA were observed at 2007 cm^{-1}, 1905 cm^{-1} and GSB was observed at 2020 cm^{-1}, 1925 cm^{-1}, and 1890 cm^{-1}. The shape of spectra at 0 ns corresponded to the T_1 spectra in the ns-μs range TR-IR measurements. Up to 1 μs, the ESA at 2007 cm^{-1} gradually red shifted to 1999 cm^{-1}. A new ESA was appeared at 1875 cm^{-1}, and the intensity of GSB at 1925 cm^{-1} was increased. Based on the discussion on the TA spectra, this spectral change is attributed to the process of OERS by BIH and the spectra after 1 μs were assigned to OERS.

Figure 6(b) (red circles) plots the ΔAbs at 1870 cm^{-1}, where one of the ESAs assigned to OERS is located, as a function of delay time. It was found that the ΔAbs increases with two distinct time constants: the components with a fast sub-microsecond process and subsequent slower process. These time constants are assigned to the two reduction processes: the reductive quenching of T_1 by BIH and the reduction of S_0 by BI・, respectively [5,19]. We conducted the least-squares fit on the data points at 1870 cm^{-1} using a double exponential function (red line in Figure 6(b)), and obtained the time constants of 170±40 ns and 3±0.8 μs for the reduction by BIH and BI・, respectively.

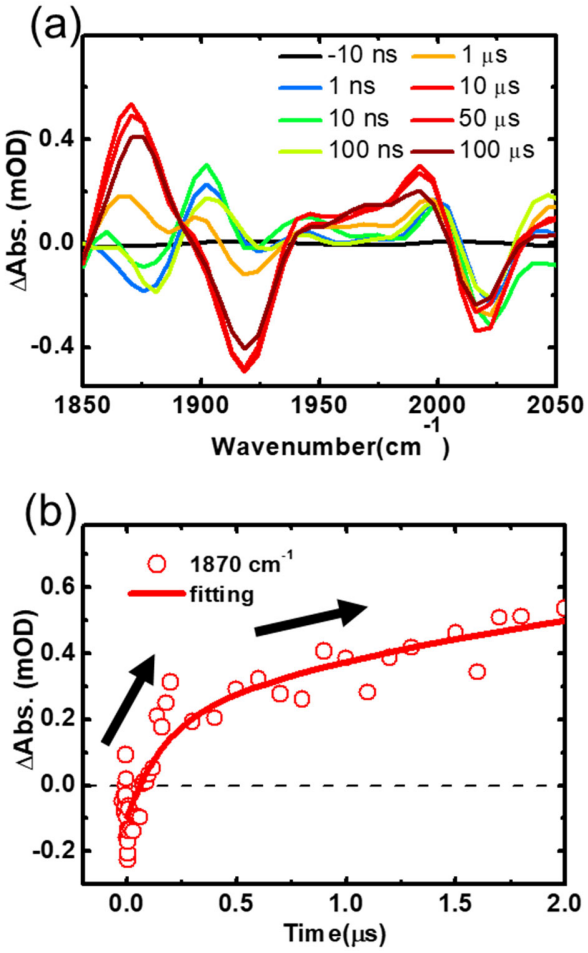

Figure 6. (a) Temporal evolution of TR-IR spectra in the ns-μs range of **ZnP-phen=Re** in a 0.1 mM DMA solution with 0.05 M BIH after photoexcitation at 410 nm. (b) Temporal profile of the TR-IR spectra at 1870 cm^{-1} (red circles) and the fitting curve using a double exponential function (red line).

To discuss the wavenumber shifts more quantitatively, we estimated the peak postions assigned to OERS by spectral deconvolution. The center positions of OERS vibrations were estimated to be 2003 cm^{-1} (Table 2) and the shift from that of S_0 is -16 cm^{-1}. This shift is rather modest compared to that in *fac*-[Re(bipyridine)$(CO)_3$Cl] by IR spectroelectrochemical measurements, -27 cm^{-1} [41,42]. In the TR-IR measurement of **Ru-Re** system, the shift of CO observed in OERS was -26 cm^{-1} [5]. Since the shift in **ZnP-phen=Re** was significantly smaller than those previously reported in [Re(bpy)$(CO)_3$Cl] and **Ru-Re**, the electron density on the Re ion in OERS of **ZnP-phen=Re** is significanlty smaller.

Table 2. Center positions determined by multi-Gaussian fit to the TR-IR spectra in the range from 1990 cm^{-1} to 2040 cm^{-1} at 100 μs for OERS, and wavenumber shifts from those in S_0, along with the correspoing values for *fac*-Re(bpy)$(CO)_3$Cl[41] and **Ru-Re**[5]**.**

	Center position	Shift from S_0
OERS	2003 cm^{-1}	-16 cm^{-1}
OERS ([Re(bpy)$(CO)_3$Cl])	1992 cm^{-1}	-27 cm^{-1}
OERS (**Ru-Re**)	1998 cm^{-1}	-26 cm^{-1}

We also measured the TR-IR spectra in the presence of BIH under CO_2 atmosphere to investigate the reaction between OERS and CO_2 and shown in Figure S7(a). Figure 7S(b) shows the temporal profile at 1870 cm^{-1}, which is assigned to OERS. Because this result is almost the

same as that without CO_2 (Figure 6) and the experimental condition that the repetition time of measurement was 1 ms is considered, we concluded that the reaction between OERS and CO_2 occurs later than 1 ms. This is consistent with the previous research on *fac*-[Re(bipyridine)$(CO)_3$Cl][5,43,44].

3.2.3. Quantum chemical calculations

We performed DFT calculations to discuss the molecular-level picture of the system. In the calculations, the open-shell UHF was used due to its charge being -1 and spin multiplicity being 2. Figure 7(a) shows the comparison of the experimental and calculated vibrational spectra, which were reasonably consistent. Figure 7(b) shows the electron distribution of singly occupied molecular orbital (SOMO). In this result, the electron distribution spans **ZnP** and the **phen** part of **phen=Re**. According to the optimized geometries, the dihedral angle between **ZnP** and **phen** in the OERS structure was 126°, which is larger than the dihedral angle of 102° in S_0. This large difference in the dihedral angle between S_0 and OERS presumably stabilize OERS and make its lifetime longer enough to proceed the next step.

Mulliken analysis was performed to examine the difference in charge density of S_0 and OERS in more detail, with the results presented in Table S1. In this data, the most negatively charged ligand is the **ZnP**, and the next one is **phen**. As can be seen from SOMO, in OERS, the electron is primarily located at the **ZnP** part and spans to the **phen** part. The smaller amount of CO peak shifts in **ZnP-phen=Re** compared to previous reports is due to the electron being located at the **ZnP** part rather than the Re metal center.

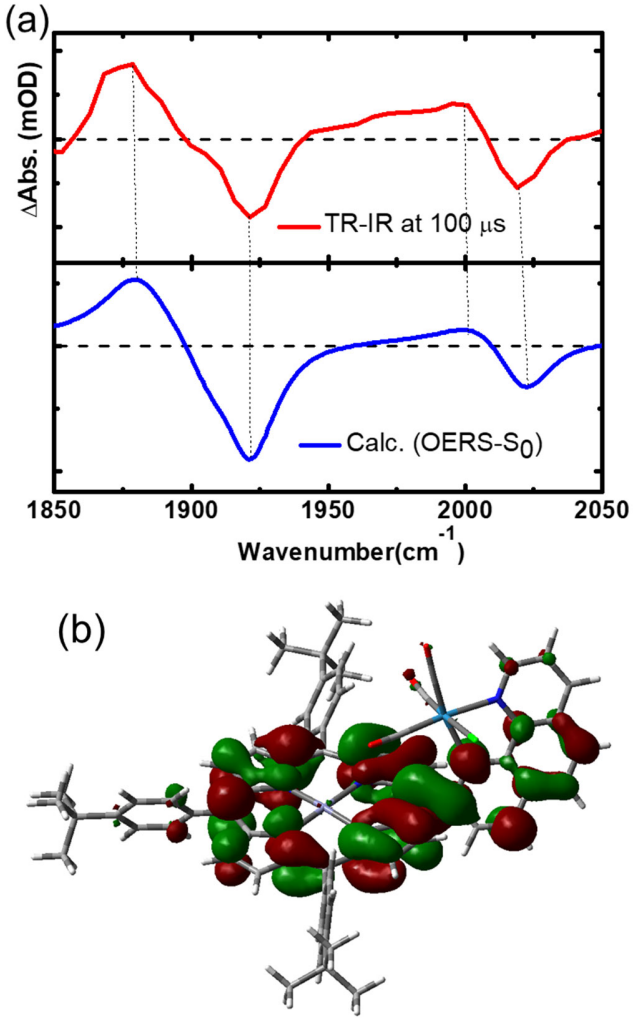

Figure 7. (a) TR-IR spectrum at 100 μs (red line) of **ZnP-phen=Re** with 0.05 M BIH and calculated difference IR spectra between OERS and S_0 (blue line) in **ZnP-phen=Re**, and (b) SOMO for OERS at the optimized geometries.

3.3. Total picture of the initial processes of CO_2 photoreduction

The initial process of **ZnP-phen=Re** after photoexcitation was clarified below (Scheme 2). Photoexcitation at 400 nm generates S_2 of **ZnP**, followed by IC to S_1 with the time constant of ~0.2 ps. Subsequently, ISC from S_1 to T_1 occurs with the time constant of ~20 ps, which is approximately 50 times faster than that of 1-2 ns observed in the pristine **ZnP**. The lifetime of T_1 is ~100 μs, indicating that T_1 has a sufficiently long lifetime as a photosensitizer. Both S_1 and T_1 shows the π-π^* transition of **ZnP** with slight π-conjugation extension to **phen** resulted from the perturbation caused by docking the **phen=Re** catalyst block. With the addition of BIH, OERS is generated by redutive quenching of T_1 with the time constant of ~170 ns. In parallel, OERS is directly generated by reduction of **ZnP-phen=Re** in the ground state by BI· with the time constant of ~3 μs. The electron in OERS is primarily located at the **ZnP** part and spans to the **phen** part.

From these results, we summarize the advantages of **ZnP-phen=Re** compared to other CO_2 photoreduction dyad catalysts using a porphyrin sensitizer. Firstly, due to the Re ion being close to **ZnP**, the ISC is accelerated and energy loss processes from S_1 such as radiative and nonradiative deactivation was efficiently suppressed. Secondly, the electron transfer from **ZnP** to **phen=Re** occurs immediately after the reduction because of the π-conjugation of **ZnP** and **phen**. Thirdly, OERS is stable because the large difference in structure between S_0 and OERS. These advantages originate from the strong electronic coupling and the congested structure thanks to the direct connection between the photosensitizer part and the catalyst part. This characteristic also makes a difference in the initial processes from the **Ru-Re** systems.

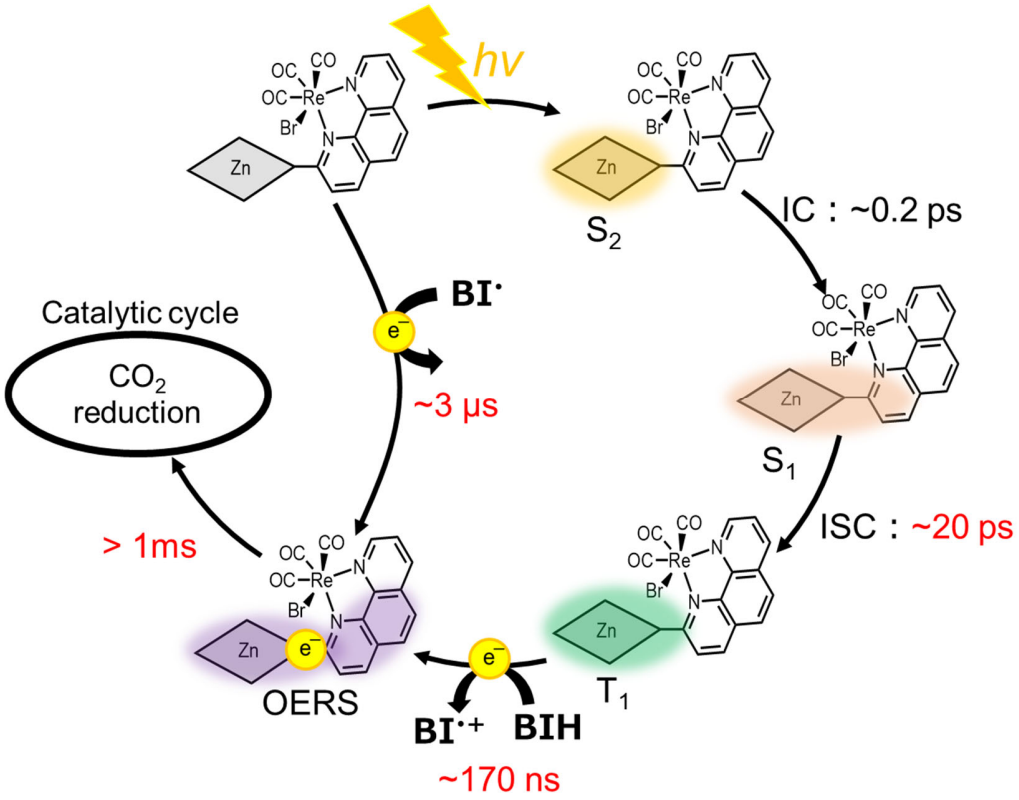

Scheme 2. Proposed mechnism of the initial process in the photocatalytic CO_2 reduction reaction using **ZnP-phen=Re**

Conclusion

We have investigated the process from photoexcitation to generation of ORES in **ZnP-phen=Re**, which is an efficient CO_2 photoreduction catalyst having zinc (II) porphyrin as a photosensitizer, using time-resolved spectroscopies, TR-IR and Vis-NIR TA, and quantum chemical calculations. Immediately after photoexcitation, after a quick IC from S_2 and S_1 within 0.2 ps, ISC from S_1 to T_1 occurs with the time constant of ~20 ps. This fast ISC compared to general porphyrins originates from the acceleration by heavy atom effect of Re ion that is located just above **ZnP**, and suppresses the energy loss processes from S_1. The charge distribution in the excited state is mostly localized on **ZnP**, that is, π-π* transition in **ZnP**. The dihedral angle between **ZnP** and **phen** is slightly changed from S_0 to S_1 but that in T_1 becomes closer to that in S_0, which causes the wavenumber shift of CO stretching vibrations in **phen=Re**. In the presence of BIH, OERS is generated via the two distinct paths: one is the reductive quenching of T_1 by BIH with the time constant of ~170 ns and the other is direct reduction of S_0 by BI• with the time constant of ~3 μs. The charge distribution in OERS spans **ZnP** and **phen**, indicating that electron transfer occurs immediately after the reduction by BIH or BI•. The fact that the dihedral angle is rotated by 24° with respect to that of S_0 would make ORES stable. The measurement under CO_2 implied that the next reaction step occurs later than 1 ms, which is the repetition time of the measurement. These characteristics on the initial process of CO_2 photoreduction were revealed by the combination method of the TR-IR, Vis-NIR TA, and quantum chemical calculations. And, based on this knowledge, novel molecular designs of dyad catalysts having a porphyrin photosensitizer would be realized.

Acknowledgements

This work was partially supported by JSPS KAKENHI (grant numbers JP20H05676, JP22H02159, JP22H02186, JP23H03833, JP23H01977, JP23H04631, JP23K20039), ENEOS Hydrogen Trust Fund, Toyota Riken Scholar, Kyushu University Platform of Inter-/Transdisciplinary Energy Research (Q-PIT) Module-Research Program, Kyushu University Integrated Initiative for Designing Future Society. The calculations were carried out using the computer resource by Research Institute for Information Technology, Kyushu University.

References

(1) Inoue, H.; Shimada, T.; Kou, Y.; Nabetani, Y.; Masui, D.; Takagi, S.; Tachibana, H. The Water Oxidation Bottleneck in Artificial Photosynthesis: How Can We Get through It? An Alternative Route Involving a Two-Electron Process. *ChemSusChem.*, **2011**, *4*, 173–179.

(2) Tamaki, Y.; Ishitani, O. Supramolecular Photocatalysts for the Reduction of CO_2. *ACS Catal.,* **2017**, *7* (5), 3394–3409.

(3) Sahara, G.; Ishitani, O. Efficient Photocatalysts for CO_2 Reduction. *Inorg, Chem.*, **2015**, *54*, 5096-5104.

(4) Lu, M.; Iz Hang, M.; Liu, J.; Chen, Y.; Liao, J.-P.; Ing-Yiy, M.; Cai, Y. U.-P.; Li, S.-L.; Lan, Y.-Q. Covalent Organic Framework Based Functional Materials:I Mportant Catalysts for Efficient CO_2 Utilization. *Angew. Chem*., **2022**, *134*, e202200003.

(5) Kamogawa, K.; Shimoda, Y.; Miyata, K.; Onda, K.; Yamazaki, Y.; Tamaki, Y.; Ishitani, O. Mechanistic Study of Photocatalytic CO_2 Reduction Using a Ru(II)-Re(I) Supramolecular Photocatalyst. *Chem. Sci*., **2021**, *12*, 9682.

(6) Ma, F.; Luo, Z.-M.; Wang, J.-W.; Aramburu-Trošelj, B. M.; Ouyang, G. Earth-Abundant-Metal Complexes as Photosensitizers in Molecular Systems for Light-Driven CO_2 Reduction. *Coord. Chem. Rev.,* **2024**, *500*, 215529.

(7) Otsuki, J. Materials Chemistry A Materials for Energy and Sustainability Rsc.Li, Materials-a Supramolecular Approach towards Light-Harvesting Materials Based on Porphyrins and Chlorophylls. *J. Mater. Chem. A*, **2018**, *6*, 6710.

(8) Kuramochi, Y.; Satake, A.; Sandanayaka, A. S. D.; Araki, Y.; Ito, O.; Kobuke, Y. Fullerene- and Pyromellitdiimide-Appended Tripodal Ligands Embedded in Light-Harvesting Porphyrin Macrorings. *Inorg. Chem.*, **2011**, *50* (20), 10249–10258.

(9) Kiyosawa, K.; Shiraishi, N.; Shimada, T.; Masui, D.; Tachibana, H.; Takagi, S.; Ishitani, O.; Tryk, D. A.; Inoue, H. Electron Transfer from the Porphyrin S_2 State in a Zinc Porphyrin-Rhenium Bipyridyl Dyad Having Carbon Dioxide Reduction Activity. *J. Phys. Chem.*, *C*, **2009**, *113* (27), 11667–11673.

(10) Gabrielsson, A.; Hartl, F.; Zhang, H.; Smith, J. R. L.; Towrie, M.; Vlček, A.; Perutz, R. N. Ultrafast Charge Separation in a Photoreactive Rhenium-Appended Porphyrin Assembly Monitored by Picosecond Transient Infrared Spectroscopy. *J. Am. Chem. Soc.,* **2006**, *128* (13), 4253–4266.

(11) Matlachowski, C.; Braun, B.; Tschierlei, S.; Schwalbe, M. Photochemical CO_2 Reduction Catalyzed by Phenanthroline Extended Tetramesityl Porphyrin Complexes Linked with a Rhenium(I) Tricarbonyl Unit. *Inorg. Chem.,* **2015**, *54* (21), 10351–10360.

(12) Windle, C. D.; George, M. W.; Perutz, R. N.; Summers, P. A.; Zhong Sun, X.; Whitwood, A. C. Comparison of Rhenium-Porphyrin Dyads for CO_2 Photoreduction: Photocatalytic

Studies and Charge Separation Dynamics Studied by Time-Resolved IR Spectroscopy. *Chem. Sci*., **2015**, *6*, 6847.

(13) Windle, C. D.; Caˆmpian, M. V. C.; Duhme-Klair, A.-K.; Gibson, E. A.; Perutz, R. N.; Schneider, J. CO_2 Photoreduction with Long-Wavelength Light: Dyads and Monomers of Zinc Porphyrin and Rhenium Bipyridinew. *Chem. Commun.,* **2012**, *48*, 8189–8191.

(14) Kitagawa, Y.; Takeda, H.; Ohashi, K.; Asatani, T.; Kosumi, D.; Hashimoto, H.; Ishitani, O.; Tamiaki, H. Photochemical Reduction of CO_2 with Red Light Using Synthetic Chlorophyll-Rhenium Bipyridine Dyad. *Chem. Lett.*, **2014**, *43*, 1383–1385.

(15) Lang, P.; Pfrunder, M.; Quach, G.; Braun-Cula, B.; Moore, E. G.; Schwalbe, M. Sensitized Photochemical CO_2 Reduction by Hetero-Pacman Compounds Linking a Re(I) Tricarbonyl with a Porphyrin Unit. *Chem. Eur. J.*, **2019**, *25* (17), 4509–4519.

(16) Kuramochi, Y.; Fujisawa, Y.; Satake, A. Photocatalytic CO_2 Reduction Mediated by Electron Transfer via the Excited Triplet State of Zn(II) Porphyrin. *J. Am. Chem. Soc.*, **2020**, *142* (2), 705–709.

(17) Kuramochi, Y.; Satake, A. Photocatalytic CO_2 Reductions Catalyzed by Meso-(1,10-Phenanthrolin-2-yl)-Porphyrins Having a Rhenium(I) Tricarbonyl Complex. *Chem. Eur. J.*, **2020**, *26* (69), 16365–16373.

(18) Kuramochi, Y.; Satake, A. Porphyrins Acting as Photosensitizers in the Photocatalytic CO_2 Reduction Reaction. *Catalysts*, **2023**, *13*. 282.

(19) Tamaki, Y.; Koike, K.; Morimoto, T.; Ishitani, O. Substantial Improvement in the Efficiency and Durability of a Photocatalyst for Carbon Dioxide Reduction Using a Benzoimidazole Derivative as an Electron Donor. *Journal of Catalysis*, **2013**, *304*, 22-28.

(20) Mukuta, T.; Fukazawa, N.; Murata, K.; Inagaki, A.; Akita, M.; Tanaka, S.; Koshihara, S. Y.; Onda, K. Infrared Vibrational Spectroscopy of $[Ru(Bpy)2(Bpm)]^{2+}$ and $[Ru(Bpy)3]^{2+}$ in the Excited Triplet State. *Inorg. Chem.*, **2014**, *53* (5), 2481–2490.

(21) Mukuta, T.; Tanaka, S.; Inagaki, A.; Koshihara, S. Y.; Onda, K. Direct Observation of the Triplet Metal-Centered State in $[Ru(Bpy)3]^{2+}$ Using Time-Resolved Infrared Spectroscopy. *ChemistrySelect*. **2016**, *1* (11), 2802–2807.

(22) Zahn, C.; Pastore, M.; Lustres, J. L. P.; Gros, P. C.; Haacke, S.; Heyne, K. Femtosecond Infrared Spectroscopy Resolving the Multiplicity of High-Spin Crossover States in Transition Metal Iron Complexes. *J. Am. Chem. Soc.* **2024**, *146*, 13, 9347-9355.

(23) Yamazaki, Y.; Ohkubo, K.; Saito, D.; Yatsu, T.; Tamaki, Y.; Tanaka, ichi; Koike, K.; Onda, K.; Ishitani, O. Kinetics and Mechanism of Intramolecular Electron Transfer in Ru(II)−Re(I) Supramolecular CO_2 −Reduction Photocatalysts: Effects of Bridging Ligands. *Inorg. Chem*., **2019**, *58*, 17, 11480-11492.

(24) Sakakibara, N.; Kamogawa, K.; Miyoshi, A.; Maeda, K.; Ishitani, O. Synergetic Effect of Ligand Modification of a Ru(II) Complex Catalyst and Ag Loading for Constructing a

Highly Active Hybrid Photocatalyst Using C_3N_4 for CO_2 Reduction. *Energy and Fuels*, **2024**, *38*, 3,2343-2350.

(25) Kamogawa, K.; Kato, Y.; Tamaki, Y.; Noguchi, T.; Nozaki, K.; Nakagawa, T.; Ishitani, O. Overall Reaction Mechanism of Photocatalytic CO_2 Reduction on a Re(I)-Complex Catalyst Unit of a Ru(II)-Re(I) Supramolecular Photocatalyst . *Chem. Sci*. **2024**, *15*, 2074-2088.

(26) Saigo, M.; Miyata, K.; Sei'ichi Tanaka, Nakanotani, H.; Adachi, C.; Onda, K. Suppression of Structural Change upon S_1 −T_1 Conversion Assists the Thermally Activated Delayed Fluorescence Process in Carbazole-Benzonitrile Derivatives. *J. Phys. Chem. Lett.,* **2019**, *10*, 10, 2475-2480.

(27) Shimoda, Y.; Miyata, K.; Saigo, M.; Tsuchiya, Y.; Adachi, C.; Onda, K. Cite As. *J. Chem. Phys.*, **2020**, *153*, 204702.

(28) Shimoda, Y.; Miyata, K.; Funaki, M.; Ehara, T.; Morimoto, T.; Nozawa, S.; Adachi, S. I.; Ishitani, O.; Onda, K. Determining Excited-State Structures and Photophysical Properties in Phenylphosphine Rhenium(I) Diimine Biscarbonyl Complexes Using Time-Resolved Infrared and X-Ray Absorption Spectroscopies. *Inorg. Chem.,* **2021**, *60* (11), 7773–7784.

(29) Mukuta, T.; Tanaka, S.; Inagaki, A.; Koshihara, S. Y.; Onda, K. Direct Observation of the Triplet Metal-Centered State in $[Ru(Bpy)3]^{2+}$ Using Time-Resolved Infrared Spectroscopy. *ChemistrySelect* **2016**, *1* (11), 2802–2807.

(30) Gaussian 03, Revision C.02, Frisch, M. J.; Trucks, G. W.; Schlegel, H. B.; Scuseria, G. E.; Robb, M. A.; Cheeseman, J. R.; Montgomery, Jr., J. A.; Vreven, T.; Kudin, K. N.; Burant, J. C.; Millam, J. M.; Iyengar, S. S.; Tomasi, J.; Barone, V.; Mennucci, B.; Cossi, M.; Scalmani, G.; Rega, N.; Petersson, G. A.; Nakatsuji, H.; Hada, M.; Ehara, M.; Toyota, K.; Fukuda, R.; Hasegawa, J.; Ishida, M.; Nakajima, T.; Honda, Y.; Kitao, O.; Nakai, H.; Klene, M.; Li, X.; Knox, J. E.; Hratchian, H. P.; Cross, J. B.; Bakken, V.; Adamo, C.; Jaramillo, J.; Gomperts, R.; Stratmann, R. E.; Yazyev, O.; Austin, A. J.; Cammi, R.; Pomelli, C.; Ochterski, J. W.; Ayala, P. Y.; Morokuma, K.; Voth, G. A.; Salvador, P.; Dannenberg, J. J.; Zakrzewski, V. G.; Dapprich, S.; Daniels, A. D.; Strain, M. C.; Farkas, O.; Malick, D. K.; Rabuck, A. D.; Raghavachari, K.; Foresman, J. B.; Ortiz, J. V.; Cui, Q.; Baboul, A. G.; Clifford, S.; Cioslowski, J.; Stefanov, B. B.; Liu, G.; Liashenko, A.; Piskorz, P.; Komaromi, I.; Martin, R. L.; Fox, D. J.; Keith, T.; Al-Laham, M. A.; Peng, C. Y.; Nanayakkara, A.; Challacombe, M.; Gill, P. M. W.; Johnson, B.; Chen, W.; Wong, M. W.; Gonzalez, C.; and Pople, J. A.; Gaussian, Inc., Wallingford CT, (2004)

(31) Scott, A. P.; Radom, L. Harmonic Vibrational Frequencies: An Evaluation of Hartree-Fock, Møller-Plesset, Quadratic Configuration Interaction, Density Functional Theory, and Semiempirical Scale Factors. *Journal of Physical Chemistry*, **1996**, *100* (41), 16502–16513.

(32) Moravec, D. B.; Lovaasen, B. M.; Hopkins, M. D. Near-Infrared Transient-Absorption Spectroscopy of Zinc Tetraphenylporphyrin and Related Compounds. Observation of Bands That Selectively Probe the S_1 Excited State. *J. Photochem. Photobiol. A Chem.*, **2013**, *254*, 20–24.

(33) Hayes, R. T.; Walsh, C. J.; Wasielewski, M. R. Competitive Electron Transfer from the S_2 and S_1 Excited States of Zinc Meso-Tetraphenylporphyrin to a Covalently Bound Pyromellitimide: Dependence on Donor-Acceptor Structure and Solvent. *J. Phys. Chem. A*, **2004**, 108, 13, 2375-2381.

(34) Mataga, N.; Taniguchi, S.; Chosrowjan, H.; Osuka, A.; Yoshida, N. Ultrafast Charge Separation and Radiationless Relaxation Processes from Higher Excited Electronic States of Directly Linked Porphyrin-Acceptor Dyads. *Photochemical and Photobiological Sciences*, **2003**, *2* (5), 493–500.

(35) Ohno, O.; Kaizu, Y.; Kobayashi, H. Luminescence of Some Metalloporphins Including the Complexes of the IIIb Metal Group. *J Chem Phys* **1984**, *82* (4), 1779–1787.

(36) Butler, J. M.; George, M. W.; Schoonover, J. R.; Dattelbaum, D. M.; Meyer, T. J. Application of Transient Infrared and near Infrared Spectroscopy to Transition Metal Complex Excited States and Intermediates. *Coord. Chem. Rev.*, **2007**, *251*, 492–514.

(37) Schoonover, J. R.; Bignozzi, C. A.; Meyer, T. J. Application of Transient Vibrational Spectroscopies to the Excited States of Metal Polypyridyl Complexes. *Coord. Chem. Rev.*, **1997**, *165*, 239–266.

(38) Kuramochi, Y.; Suzuki, Y.; Asai somyo.; Suzuki, T.; Iwama, H.; Asano, M. S.; Satake, A. Photocatalytic CO_2 reduction sensitized by a special-pair mimic porphyrin connected with a rhenium(I) tricarbonyl complex. *Chem. Sci*., **2023**, *14*, 8743–8765.

(39) Irikura, M.; Tamaki, Y.; Ishitani, O. Development of a Panchromatic Photosensitizer and Its Application to Photocatalytic CO_2 Reduction. *Chem. Sci*., **2021**. *12*, 13888-13896.

(40) Hori, H.; Johnson, F. P. A.; Koike, K.; Ishitani, O.; Ibusuki, T. Efficient Photocatalytic CO_2 Reduction Using $[Re(bpy)(CO)_3\{P(OEt)_3\}]^+$. *J. Photochem. Photobio. A Chem.,* **1996**, *96*, 171–174.

(41) Johnson, F. P. a; George, M. W.; Hartl, F.; Turner, J. J. Electrocatalytic Reduction of CO_2 Using the Complexes $[Re(bpy)(CO)_3L]^n$ (n=+1, L=$P(OEt)_3$, CH_3CN;n=0, L=Cl^-, Otf^-; bpy=2,2'-Bipyridine; Otf^-= CF_3SO_3) as Catalyst Precursors: Infrared Spectroelectrochemical Investigation. *Organometallics*, **1996**, *15* (15), 3374–3387.

(42) Smieja, J. M.; Kubiak, C. P. Re(bipy-tBu)$(CO)_3$Cl-Improved Catalytic Activity for Reduction of Carbon Dioxide: IR-Spectroelectrochemical and Mechanistic Studies. *Inorg. Chem.,* **2010**, *49* (20), 9283–9289.

(43) Kou, Y.; Nabetani, Y.; Masui, D.; Shimada, T.; Takagi, S.; Tachibana, H.; Inoue, H. Direct Detection of Key Reaction Intermediates in Photochemical CO_2 Reduction Sensitized by a Rhenium Bipyridine Complex. *J. Am. Chem. Soc.,* **2014**, *136* (16), 6021–6030.

(44) Kou, Y.; Nabetani, Y.; Nakazato, R.; Pratheesh, N. V.; Sato, T.; Nozawa, S.; Adachi, S. ichi; Tachibana, H.; Inoue, H. Mechanism of the Photoreduction of Carbon Dioxide Catalyzed by the Benchmarking Rhenium Dimethylbipyridine Complexes; Operando Measurements by XAFS and FT-IR. *J. Catal.,* **2022**, *405*, 508–519.